Complex rare-earth tetrelides, $RE_5(Si_xGe_{1-x})_4$: New materials for magnetic refrigeration and a superb playground for solid state chemistry

Gordon J. Miller

Received 13th February 2006
First published as an Advance Article on the web 19th May 2006
DOI: 10.1039/b208133b

A "giant magnetocaloric effect" discovered in 1997 for $Gd_5Si_2Ge_2$ near room temperature has triggered optimism that environmentally-friendly, solid-state magnetic refrigeration may be viable to replace gas-compression technology in the near future. $Gd_5Si_2Ge_2$ is one member of an extensive series of rare-earth compounds, $RE_5(Si_xGe_{1-x})_4$. Due to the complexity of their structures and flexibility associated with chemical compositions, this series is an attractive "playground" to study the interrelationships among composition, structure, physical properties and chemical bonding. This *tutorial review*, which is directed toward students and researchers interested in structure–property relationships in solids, summarizes recent efforts concerning the synthesis, structure, physical properties, chemical bonding and chemical modifications of $RE_5(Si_xGe_{1-x})_4$. A brief history of refrigerants, to present certain motivating factors for this research effort, as well as a brief overview of the magnetocaloric effect serves to introduce this review.

Why pursue magnetic refrigeration?

Refrigeration at ambient conditions currently relies nearly exclusively on gas-compression technology. The principle was first demonstrated by William Cullen at the University of Glasgow in 1748, and John Gorrie, an American physician, received the first US patent for mechanical refrigeration in 1851.[1] The early refrigerators used air as a coolant, but developments during the second half of the nineteenth century led to the use of ammonia, sulfur dioxide and methyl chloride, which have desirably high latent heats of vaporization while boiling in the range −40° to −10 °C at 1 atm pressure.[2] However, these gases are toxic and/or corrosive and after a series of fatal industrial accidents in the 1920s, Frigidare (then a division of General Motors) and DuPont collaborated on identifying new, nontoxic fluids for refrigeration and air conditioning. This work led to the discovery of halocarbons, chlorofluorocarbons (CFCs), of which CF_2Cl_2 was patented under the name "Freon." These fluids showed desirable thermochemical properties and were nontoxic and odorless. Some fifty years later, in 1973, James Lovelock reported finding trace amounts of these gases in the atmosphere, and then, Sherwood Rowland and Mario Molina predicted that CFC molecules could reach the stratosphere where chlorine radicals generated from these molecules could consume ozone. 1985 marked the discovery of the "ozone hole" and coincided with the Vienna Convention that established mechanisms for international cooperation in research of the effects of ozone depleting chemicals (ODCs). On the basis of the Vienna Convention, the *Montreal Protocol on Substances that Deplete the Ozone Layer* was signed by 24 countries and the European Economic Community in 1987, which called for these nations to phase down the use of CFCs, halons and other man-made ODCs. Therefore, there exist strong environmental and political motivations for identifying alternative refrigeration technologies to completely phase out the use of these fluids.

Recent scientific and engineering efforts are directed toward thermoelectric or thermomagnetic cooling, both of which are considered environmentally friendly. Conventional vapor-cycle refrigeration achieves cooling efficiencies approaching 40% of the theoretical (Carnot) limit. Thermoelectric cooling, which relies on the Peltier effect to create a heat difference through an applied potential across two dissimilar metals or semiconductors, suffers from relatively low efficiency—*ca.* 10% of the Carnot limit.[3] Nevertheless, Peltier cooling can be advantageous in small volumes, as in integrated circuits, but does not seem well suited for larger scale cooling/refrigeration.

Department of Chemistry, Iowa State University and Ames Laboratory, US Department of Energy, Ames, Iowa 50011, USA

Gordon J. Miller

Gordon J. Miller is Professor of Chemistry at Iowa State University and Associate Scientist in the Ames Laboratory. He joined Iowa State in 1990 after completing a PhD in Chemistry under the guidance of Prof. Jeremy K. Burdett at the University of Chicago in 1986 and a post-doctoral appointment at the Max-Planck-Institute for Solid State Research in Stuttgart, Germany. In 1995, he received the Exxon Faculty Fellowship in Solid State Chemistry and served as Editor of the Journal of Alloys and Compounds from 1998–2005. He was Chemistry Department Chair at Iowa State from 2002–2005. His group's research interests include experimental and theoretical studies of complex intermetallic systems.

Magnetic refrigeration (thermomagnetic cooling) has been shown to achieve cooling efficiencies of 60% of the theoretical limit, but with currently available magnetic materials, this efficiency is only realized in high magnetic fields of 5 Tesla.[4] Nevertheless, the potential for higher efficiencies can create savings in cost and energy consumption. During the past decade, there has been tremendous worldwide effort to identify materials that can be used for magnetic refrigeration, especially under ambient conditions. One important class, the rare-earth (RE) tetrelides, $RE_5(Si_xGe_{1-x})_4$, has excited both the scientific and engineering communities for their extraordinarily strong magnetic responses and possible applications in magnetic refrigeration (the term ''tetrelide'' corresponds to Group 14/IVB elements because they typically form four bonds to nearest neighbor main group elements; we also use the symbol 'Tt' for tetrelide in this article).

The magnetocaloric effect

Using magnetic materials for refrigeration relies on the *magnetocaloric effect* (MCE), which is most easily observed as a temperature change of the material caused during an adiabatic change of an applied magnetic field on the material.[5] Warburg discovered this effect in iron in 1881. Then, some 30 years later, W. F. Giauque and P. Debye independently predicted, and W. F. Giauque and D. P. McDougal utilized the effect by *adiabatically demagnetizing* paramagnetic gadolinium sulfate hydrate, $Gd_2(SO_4)_3{\cdot}8H_2O$, to reach the lowest temperature at that time, *i.e.* 0.25 K. For this process, illustrated in Fig. 1, a sample of a paramagnetic material, cooled to *ca.* 1 K, is magnetized by a strong magnetic field H (and surrounded by helium gas to provide thermal contact with a cold reservoir). Heat flows out of the sample as the magnetic moments align with the applied field. As the thermal contact is removed by evacuating the helium, the applied field is reduced quickly to zero—there is no heat flow in this step and the material adopts a state of lower temperature. For paramagnetic substances with noninteracting magnetic moments, the magnetic entropy is a function of H/T only. Therefore, for an adiabatic process ($\Delta S = 0$), H/T remains constant and $T_2 = (H_2/H_1)T_1$. Thus, when a paramagnetic material is demagnetized adiabatically ($H_2 < H_1$), magnetic ions redistribute among available states and the temperature drops ($T_2 < T_1$) until the internal constraining forces produce a state at low field with the same entropy as produced by the higher field at the initial, higher temperature. This ''rule'' breaks down as T approaches 0 K because it violates the third law of thermodynamics. W. F. Giauque received the Nobel Prize in Chemistry in 1949 for his discoveries and, particularly, these concepts, which reliably achieve milliKelvin temperatures. Then, in the 1960s, $PrNi_5$ was used in nuclear demagnetization refrigeration by using the magnetic dipoles of the nuclei to achieve microKelvin temperatures—to date, adiabatic demagnetization remains the sole means to achieve such ultra-low temperatures, *i.e.*, $T < 10^{-3}$ K.

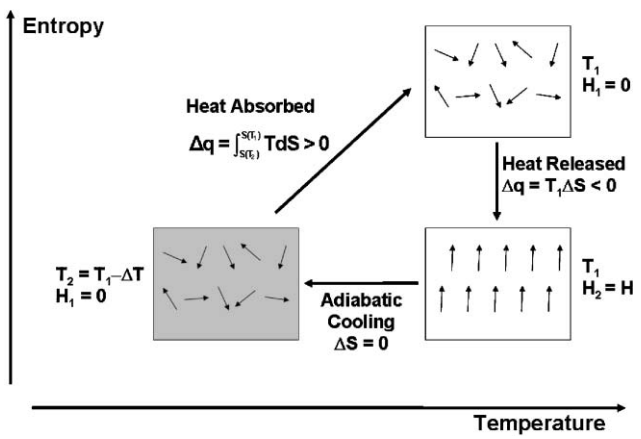

Fig. 1 Entropy–temperature schematic of the adiabatic demagnetization process and its application to magnetic refrigeration. A magnetic material starts at temperature T_1 in the absence of a magnetic field ($H_1 = 0$). The sample is then magnetized isothermally ($H_2 = H > 0$); heat is released to the reservoir ($\Delta q = T_1\Delta S$). Then, the field is turned off adiabatically ($\Delta S = 0$) and the magnetic disorder increases—the material cools to temperature $T_2 = T_1 - \Delta T$. To finish the cycle, heat is absorbed by the material to reach the initial state.

Two important measures of the MCE are the *isothermal magnetic entropy change*, $\Delta S_m(T, \Delta H)$ and the *adiabatic temperature change*, $\Delta T_{ad}(S, \Delta H)$, when the system is exposed to two different magnetic fields ($\Delta H = H_2 - H_1$; typically $H_1 = 0$ T).[6] They are readily extracted by plotting $S(T, H)$ curves for the different magnetic fields: $\Delta S_m(T, \Delta H) = S(T, H_2) - S(T, H_1)$ and $\Delta T_{ad}(S, \Delta H) = T(S, H_2) - T(S, H_1)$. As Fig. 2 illustrates, if H_2 is larger than H_1, then typically $\Delta S_m(T, \Delta H) < 0$, because there is a greater degree of magnetic order in a larger applied field, and $\Delta T_{ad}(S, \Delta H) > 0$. Both MCE parameters are typically plotted as a function of temperature; since S is a single-valued function of T, then the adiabatic temperature change can also be expressed as a function of temperature, *i.e.*, $\Delta T_{ad}(T, \Delta H)$. These characteristics are determined experimentally either directly by thermometry (directly measuring $\Delta T_{ad}(\Delta H)$) or indirectly by heat capacity measurements under different applied magnetic fields, which provides $S(T, H_i)$ curves, or by different magnetization isotherms, *i.e.*, $M(H, T_j)$ curves. The magnetic entropy change directly characterizes the cooling capacity of the magnetic material, while the adiabatic temperature change indirectly characterizes the cooling capacity and the temperature

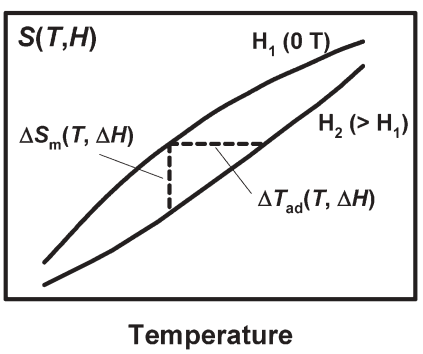

Fig. 2 Qualitative diagram of the two important characteristics of MCE as obtained from $S(T, H)$ curves. Two different magnetic fields produce different entropy curves. The isothermal magnetic entropy change, $\Delta S_m(T, \Delta H)$, and the adiabatic temperature change, $\Delta T_{ab}(T, \Delta H)$, are shown.

difference between the cold and hot ends of the refrigerator. Both parameters are important thermodynamic and engineering characteristics.

To understand what influences the magnitudes of these two characteristics in materials, we can analyze the entropy function, $S(T, p, H)$, assuming continuous thermodynamic variables. In a magnetic solid, the total entropy is the sum of electronic, lattice and magnetic entropies, *i.e.*, $S = S_{el} + S_{lat} + S_m$. For the time being, we will not consider magnetoelastic interactions, which establish a relationship among S_{el}, S_{lat}, and S_m. In this case, we have $S_{el}(T, p)$ and $S_{lat}(T, p)$ but $S_m(T, p, H)$; only the magnetic entropy depends on magnetic field. Since entropy is a state function, the total differential for a closed system under constant pressure is

$$dS = \left(\frac{\partial S}{\partial T}\right)_H dT + \left(\frac{\partial S}{\partial H}\right)_T dH. \quad (1)$$

Using the following equations of state with respect to the Gibbs free energy, $S(T, H) = -(\partial G/\partial T)_H$ and $M(T, H) = -(\partial G/\partial H)_T$, the resulting Maxwell's equation is $(\partial S/\partial H)_T = (\partial M/\partial T)_H$, and eqn (1) becomes

$$dS = \left(\frac{\partial S}{\partial T}\right)_H dT + \left(\frac{\partial M}{\partial T}\right)_H dH = \left(\frac{C_p(T,H)}{T}\right)_H dT + \left(\frac{\partial M}{\partial T}\right)_H dH, \quad (2)$$

where $C_p(T, H)$ is the heat capacity under constant pressure. Therefore, for an adiabatic process ($dS = 0$), we find the adiabatic temperature change to be

$$\Delta T_{ad}(S,\Delta H) = T(S,H_2) - T(S,H_1) = -\int_{H_1}^{H_2} \left(\frac{T}{C_p(T,H)}\right)_H \left(\frac{\partial M}{\partial T}\right)_H dH, \quad (3)$$

and the isothermal magnetic entropy change is

$$\Delta S_m(T,\Delta H) = S(T,H_2) - S(T,H_1) = \int_{H_1}^{H_2} \left(\frac{\partial M}{\partial T}\right)_H dH. \quad (4)$$

What influences the size of the magnetocaloric effect? According to eqn (3) and (4), materials whose magnetization changes rapidly with temperature will have physically significant values for ΔT_{ad} and ΔS_m. Such large $(\partial M/\partial T)_H$ values occur in two distinct cases: (a) Curie paramagnetic materials at low temperatures; and (b) ferromagnetic materials near their magnetic ordering temperatures. Curie paramagnets show magnetization in the presence of a magnetic field that is proportional to H/T, so $(\partial M/\partial T)_H$ is proportional to $-H/T^2$, which has its largest values at low temperatures. For example, for a paramagnetic Gd^{3+} salt exposed to a field that ranges from 0 to 5 T, $\Delta S_m = -0.022$ J mol^{-1} K^{-1} at 300 K, but -78.8 J mol^{-1} K^{-1} at 5 K. Paramagnetic, rare-earth compounds are optimal materials due to their large effective moments, but recent theoretical efforts suggest that frustrated antiferromagnets involving 3d transition metal ions may show a competitive MCE at low temperature.[7] On the other hand, ferromagnetic materials show critical behavior just below the Curie temperature T_C according to the relation between magnetization and temperature, $M(T) \approx (T_C - T)^{\beta}$, where $\beta \leqslant 0.5$ so that $(\partial M/\partial T)_H$ approaches $-\infty$ as T approaches T_C from below. At temperatures above and well below T_C, $(\partial M/\partial T)_H$ is small and approaches zero: at low temperatures $M(T) \rightarrow M(0)(1 - (T/T_C)^{3/2})$. Therefore, ΔT_{ad} and ΔS_m will show a maximum at T_C for ferromagnets. Fig. 3 illustrates $S(T, H)$, $-\Delta S_m(T, \Delta H)$ and $\Delta T_{ad}(T, \Delta H)$ curves for Gd, which shows the maximum in the MCE parameters at the Curie temperature[8]

Typical magnetic order–disorder phase transitions are "second order," *i.e.*, continuous, symmetry-breaking transitions as in Gd. Therefore, there is a discontinuity in $(\partial S/\partial T)_H$, which commonly gives a λ-transition in the temperature-dependent heat capacity curve. Nevertheless, the following relation for the isothermal magnetic entropy change always holds:

$$\Delta S_m(T) = S(T,H_2) - S(T,H_1) = \int_0^T \frac{C_p(T,H_2) - C_p(T,H_1)}{T} dT = \int_0^T \frac{\Delta C_p(T,\Delta H)}{T} dT \quad (5)$$

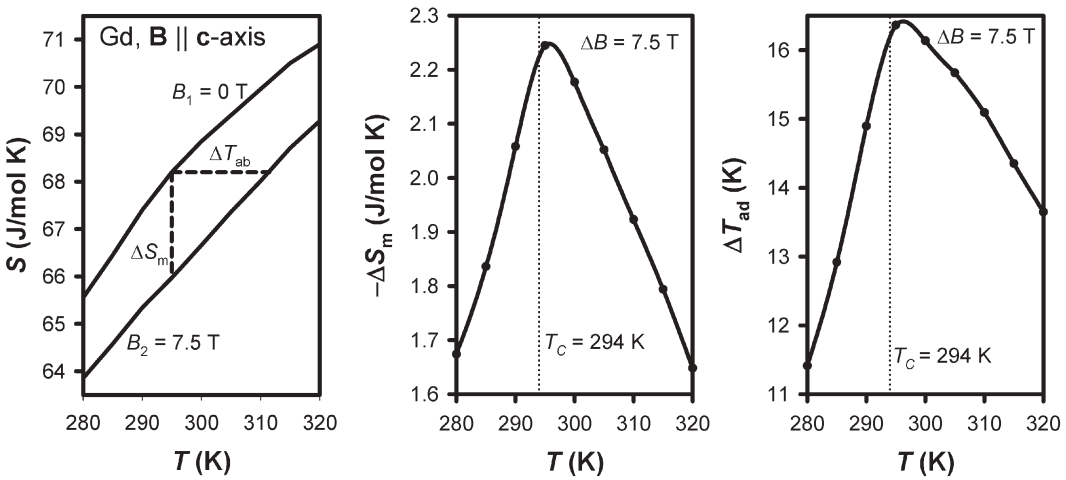

Fig. 3 $S(T, H)$, $-\Delta S_m(T, \Delta H)$ and $\Delta T_{ad}(T, \Delta H)$ curves for Gd measured with magnetic fields applied parallel to the crystallographic *c*-axis of the hexagonal unit cell. The magnetic field difference is 7.5 T; entropies are expressed in units of J mol^{-1} K^{-1}. The Curie temperature of 294 K for Gd is noted on the MCE curves. Data for these curves were taken from ref. 8.

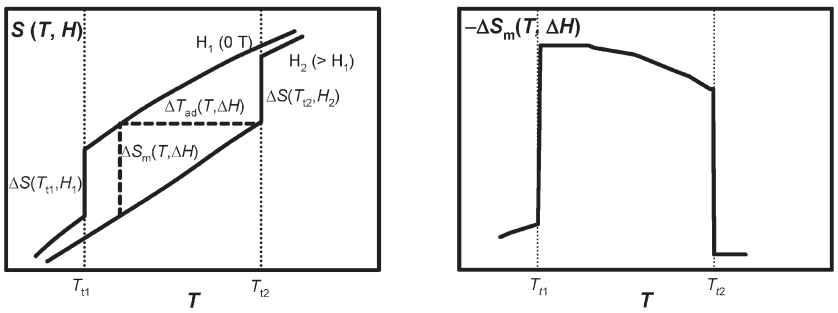

Fig. 4 (Left) Qualitative diagram of the two important characteristics of MCE as obtained from $S(T, H)$ curves when a first-order phase transition occurs. Two different magnetic fields produce different entropy curves; the transition temperature is also affected. The isothermal magnetic entropy change, $\Delta S_m(T, \Delta H)$, and the adiabatic temperature change, $\Delta T_{ab}(T, \Delta H)$, are shown. (Right) Qualitative plot of the $-\Delta S_m(T, \Delta H)$ curve resulting from the $S(T, H_1)$ and $S(T, H_2)$ curves above. Note the difference in qualitative appearance from that in Fig. 3 for Gd, where no first-order transition occurs.

which requires analyzing how heat capacity varies with magnetic field. For $\Delta H > 0$, $\Delta C_p(T, \Delta H)$ must be negative so that $\Delta S_m(T) \leqslant 0$. Furthermore, since $|\Delta S_m(T)|$ decreases with increasing temperature above the Curie temperature in ferromagnets (see Fig. 3 for Gd), there must be a change of sign in $\Delta C_p(T,\Delta H)$ above T_C.

If there is a first-order phase transition associated with the magnetic transition, then ΔS_m can take measurable and potentially applicable values associated with latent heat. Consider a first-order transition at T_{t1}, which is seen as a discontinuity in the $S(T, H_1)$ curve at T_{t1} in Fig. 4. Under a larger applied field H_2, this transition will be shifted to higher temperature, T_{t2}. Therefore, for temperatures between T_{t1} and T_{t2}, we see that the isothermal entropy change is

$$\Delta S(T) = \int_0^T \frac{C_p(T,H_2) - C_p(T,H_1)}{T}\,\mathrm{d}T - \Delta S(T_{t1},H_1) \quad (6)$$

where $\Delta S(T_{t1}, H_1) = \Delta E(T_{t1}, H_1)/T_{t1}$. Below T_{t1} and above T_{t2}, $\Delta S(T)$ will adopt smaller values according to eqn (5). Such transitions exhibit a so-called ''giant magnetocaloric effect'' that can lead to appreciable heat transfer at temperatures well above 0 K.[8,9]

Such first-order phase transitions can involve either a structural transformation or a discontinuous change in phase volume, *i.e.*, a strong magnetoelastic interaction, which provides some latent heat, $\Delta E(T_t)$, that impacts the electronic, lattice and magnetic contributions to the entropy. These first-order effects were first described phenomenologically by Bean and Rodbell.[10] Their model was expanded into the coupled-magnetic-lattice model,[11] which considers the dependence of exchange interactions on interatomic distance within a mean-field approximation by coupling the Curie temperature to a volume change: $T_C = T_0(1 + \beta\omega)$, where $\omega = (V - V_0)/V_0$ represents the relative change in unit cell volume and β, T_0 are empirical parameters. In this model, the Gibbs free energy is expressed as the sum of five terms (σ = scaled magnetization = M/M_{sat}, $0 \leqslant \sigma \leqslant 1$; κ = volume compressibility): (i) the Zeeman enthalpy, $-HM_{sat}\sigma$; (ii) the exchange enthalpy, $-\frac{1}{2}NkT_C\sigma^2$; (iii) the elastic enthalpy, $\omega^2/2\kappa$; (iv) the pressure–volume term, $p\omega$; and (v) the entropy term, $-TS(T, \omega, \sigma)$, where $S(T, \omega, \sigma) = S_{el}(T, \omega, \sigma) + S_{lat}(T, \omega, \sigma) + S_m(T, \omega, \sigma)$. Therefore,

$$G(T, \sigma) = -HM_{sat}\sigma - \tfrac{1}{2}NkT_C\sigma^2 + \omega^2/2\kappa + p\omega - TS(T, \omega, \sigma). \quad (7)$$

Minimizing the free energy with respect to volume (ω), and then to the scaled magnetization (σ) results in a series of $\sigma(T, H; \eta)$ curves, whose characteristics depend on an order parameter η ($\eta = NkT_0\kappa\beta^2$, a dimensionless quantity). Restricting the scaled magnetization to be a single-valued function of temperature gives first-order transitions for $\eta > 1$, but second-order transitions for $\eta < 1$. This model has been successfully applied to a number of different materials to interpret the $\Delta S_m(T, \Delta H)$ and $\Delta T_{ad}(T, \Delta H)$ curves using just a few parameters.[11]

In 1997, Pecharsky and Gschneidner reported a giant MCE in the ternary compound, $Gd_5Si_2Ge_2$ near 276 K, during a systematic study of rare-earth compounds showing Curie temperatures near room temperature.[12] According to both adiabatic temperature changes and isothermal magnetic entropy changes, $Gd_5Si_2Ge_2$ shows extraordinary behavior compared to elemental Gd (see Fig. 5). Since this discovery, the MCE has been studied for a number of different ferromagnetic phases showing Curie temperatures near room temperature,[8,9,13] for example, $MnFeP_{1-x}As_x$, $La(Fe_{1-x}Si_x)_{13}H_n$, ''Ni_2MnGa'' and MnAs (see Table 1). In ''Ni_2MnGa'' the ferromagnetic ordering and structural transitions are decoupled; magnetic ordering occurs in the high-symmetry structure, then the structural transition ensues.[13] In all cases, a ferromagnetic–paramagnetic transition occurs as well as some form of structural change—either a significant change in molar volume or in local chemical bonding through distortion of the unit cell, which contribute to $\Delta S(T_t)$ terms in eqn (6). In order to study MCE thoroughly, scientific work involves a combination of careful synthesis including chemical substitutions, thorough temperature-dependent structural characterization, physical property measurements and electronic structure calculations—the $RE_5(Si_xGe_{1-x})_4$ system allows numerous opportunities. One note about units: chemists normally report entropy in units of J mol^{-1} K^{-1}. For characterization of MCE, engineers find J kg^{-1} K^{-1}

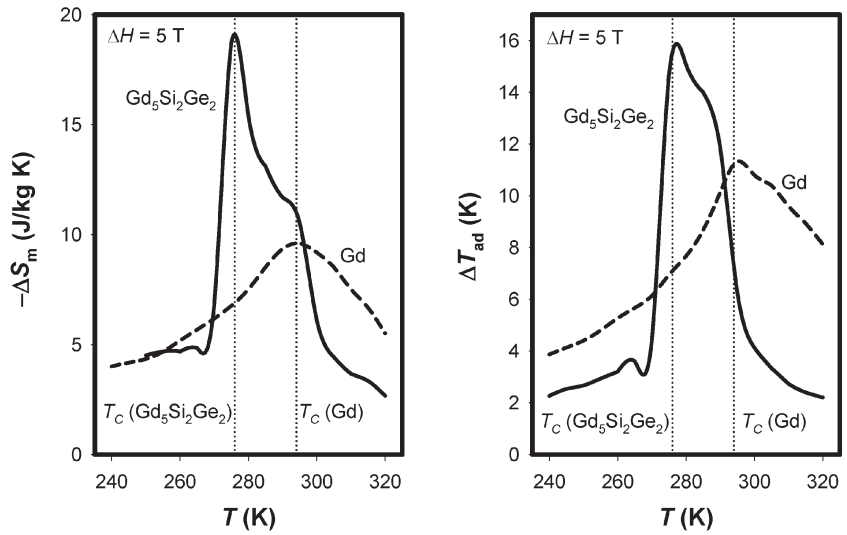

Fig. 5 MCE curves comparing $Gd_5Si_2Ge_2$ and Gd. (Left) $-\Delta S_m(T, \Delta H = 5\ T)$ curves; and (right) $\Delta T_{ad}(T, \Delta H = 5\ T)$ curves. The Curie temperatures of 276 and 294 K, respectively, for $Gd_5Si_2Ge_2$ and Gd are noted on the MCE curves. Data for these curves were taken from ref. 12.

Table 1 Summary of important MCE characteristics for several MCE materials with Curie temperatures T_C near room temperature.[9,13] Systems are listed in order of increasing T_C. $-\Delta S_m(\Delta H = 2\ T)$ are given in three different units. Please see ref. 9 for an extensive review and critical analysis of these materials

Compound	T_C (K)	ΔT_{ad}/K; (ΔH = 2T)	$-\Delta S_m$/J mol^{-1} K^{-1} (ΔH = 2 T)	$-\Delta S_m$/J kg^{-1} K^{-1} (ΔH = 2 T)	$-\Delta S_m$/mJ cm^{-3} K^{-1} (ΔH = 2 T)
$Gd_5Si_2Ge_2$	276	7.2	15.8	15.9	120
$La(Fe_{0.89}Si_{0.11})_{13}H_{1.3}$	291	7.0	19.8	24.0	171.3
Gd	294	5.8	0.8	5.1	40.3
$MnFeP_{0.45}As_{0.55}$	302	3.0	2.5	15.1	109.6
$Fe_{0.49}Rh_{0.51}$	316	8.4	1.8	22.5	110.8
MnAs	318	4.9	4.2	32.6	221
$Ni_{54.8}Mn_{20.2}Ga_{25}$	351	1.0	0.9	15.5	121

and mJ cm^{-3} K^{-1} as units that provide transparent comparisons for engineering applications.[9] Thus, conversions among these different units require knowledge of correct chemical formulas and densities, which are often available from X-ray diffraction studies.

Survey of $RE_5(Si_xGe_{1-x})_4$ systems

In fact, $Gd_5Si_2Ge_2$ is one of a nearly continuous series of compounds $Gd_5(Si_xGe_{1-x})_4$ for $0 \leqslant x \leqslant 1$, *i.e.*, between Gd_5Ge_4 and Gd_5Si_4. This series, first reported by Holtzberg and coworkers at IBM in the late 1960s, shows interesting variations in crystal lattices and magnetic properties with changes in composition.[14] One surprising result of the Holtzberg work was that the Curie temperatures for the Si-rich examples exceeded the Curie temperature of ferromagnetic Gd. This result remains an unsolved scientific question. The discovery of a giant MCE in $Gd_5Si_2Ge_2$ in 1997 triggered renewed scientific and engineering interest in this and related compounds.[12] Most of the work during the past ten years has focused on $Gd_5(Si_xGe_{1-x})_4$, but other rare-earth systems are gaining increasing interest to understand the fundamental chemistry and physics of this rich system. The remainder of this review will emphasize certain important observations and interpretations among various RE_5Tt_4, with an emphasis on the Gd examples.

Fig. 6 illustrates a temperature–composition (T–x) phase diagram for $Gd_5(Si_xGe_{1-x})_4$, which summarizes a great deal of crystallographic and magnetic measurements.[15] This T–x phase diagram shows that the magnetic transitions vary systematically with composition and that they occur with changes in crystal structure for the Ge-rich examples, *i.e.*, $x \leqslant 0.5$. Throughout this series, the low temperature system is ferromagnetic with an orthorhombic, Gd_5Si_4-type structure. In the Si-rich region ($x \geqslant 0.575$), $Gd_5(Si_xGe_{1-x})_4$ exhibit ferromagnetic–paramagnetic transitions at temperatures that exceed the Curie point of elemental Gd (T_C = 294 K), and increase slightly with increasing Si composition, but occur without a structural transformation—both structures across the magnetic transition adopt the orthorhombic Gd_5Si_4-type. On the Ge-rich side ($x \leqslant 0.50$), there is a significant change in Curie temperature with x and there are three distinct regions: (i) $0 \leqslant x \leqslant 0.30$; (ii) $0.30 \leqslant x \leqslant 0.40$; and (iii) $0.40 \leqslant x \leqslant 0.503$.[15] Throughout this range, structural changes accompany the magnetic transitions and the Curie temperatures increase essentially linearly as x increases. For $0.40 \leqslant x \leqslant 0.503$, the ferromagnetic–paramagnetic transition occurs with an orthorhombic–monoclinic (Gd_5Si_4-type to $Gd_5Si_2Ge_2$-type) structure

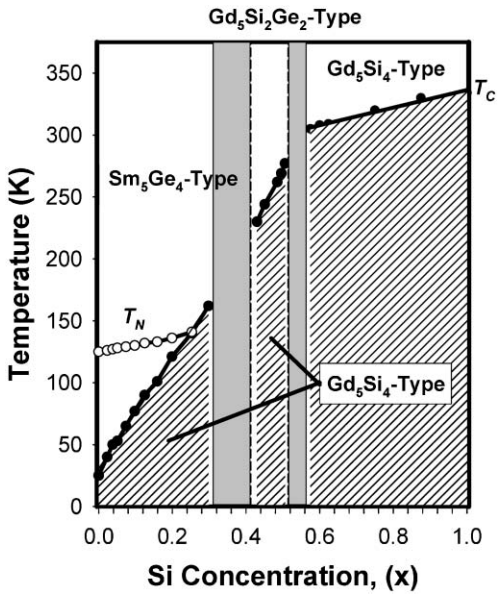

Fig. 6 Temperature–composition phase diagram for $Gd_5(Si_xGe_{1-x})_4$. Crystal structure types and magnetic characteristics are indicated as a function of Si concentration. The solid lines connecting black points correspond to the experimental Curie temperatures; solid lines connecting open points correspond to experimental Néel temperatures for Ge-rich examples. Shaded region is entirely ferromagnetic; open regions are paramagnetic. Two gray areas correspond to two-phase regions in this diagram. Data for this figure come from ref. 15.

change.[16] The structural changes from the orthorhombic, Gd_5Si_4-type at low temperatures to the monoclinic, $Gd_5Si_2Ge_2$-type at higher temperatures for this region are unusual due to the intrinsic entropy differences of the two crystal lattices because the lower symmetry crystal class, monoclinic, would be preferred at lower temperature. However, this transition is associated with a change in magnetic order. Further examination of $Gd_5Si_2Ge_2$ when it is annealed between *ca.* 600 and 1000 K shows a transformation to the Gd_5Si_4-type crystal structure and partial decomposition.[15] This orthorhombic structure remains on cooling, but can be converted back to the monoclinic form when heated above 1200 K—such experiments indicate that the monoclinic phases may be metastable at room temperature. In addition, the monoclinic to orthorhombic Gd_5Si_4-type transformation can be established in $Gd_5Si_2Ge_2$ at between 10 and 20 kbar pressure.[17] For $x \leqslant 0.30$, a different structural change takes place at the Curie temperature from one orthorhombic structure into another (Gd_5Si_4-type to Sm_5Ge_4-type†). Moreover, the transition actually corresponds to a ferromagnetic–ferrimagnetic state (or a suppressed antiferromagnetic state) until the Néel temperature *ca.* 130–140 K. Furthermore, transformations between the two orthorhombic structure types can be driven by an external magnetic field in Gd_5Ge_4 and $Gd_5Si_{0.4}Ge_{3.6}$.[18,19] Finally, the range $0.30 \leqslant x \leqslant 0.40$ is a two-phase region, showing a mixture of orthorhombic Sm_5Ge_4-type and monoclinic $Gd_5Si_2Ge_2$-type structures at room temperature that transform into two different Gd_5Si_4-type cells at low temperatures. Two phases have been observed in powder X-ray diffraction as well as in single crystal and electron diffraction experiments for $Gd_5Si_{1.5}Ge_{2.5}$ ($x = 0.375$), which indicates the microscopic nature of this two-phase region: within a single specimen, there can be sufficient concentration gradients in Si/Ge distributions to create these two phases.[20] We will discuss further details of the chemical structures and magnetic properties of $Gd_5(Si_xGe_{1-x})_4$ in later sections of this review.

Similar T–x phase diagrams have emerged for other rare-earth systems, *e.g.*, $Tb_5(Si_xGe_{1-x})_4$,[21] $Er_5(Si_xGe_{1-x})_4$,[22] $Y_5(Si_xGe_{1-x})_4$,[23] and, most recently, $Yb_5(Si_xGe_{1-x})_4$,[24] which shows mixed valence behavior. Selected $RE_5(Si_xGe_{1-x})_4$ compounds for RE = La, Pr, Nd, Tb, Dy and Lu have been reported as well.[25] However, several $RE_5(Si_xGe_{1-x})_4$ remain to be fully explored: no examples are reported for RE = Pm and Eu, while only binary RE_5Si_4 or RE_5Ge_4 have been examined for RE = Ce, Sm and Tm. At ambient temperature, four structure types exist for the $RE_5(Si_xGe_{1-x})_4$ systems[25]: (a) the tetragonal Zr_5Si_4-type found for the light lanthanide, silicon-rich cases; (b) the orthorhombic Sm_5Ge_4-type observed for the germanium-rich examples throughout the rare-earth series; (c) the monoclinic $Gd_5Si_2Ge_2$-type seen at intermediate Si and Ge compositions for the rare-earth atoms of intermediate size including yttrium (Pr–Er); and (d) the orthorhombic Gd_5Si_4-type occurring for silicon-rich heavy lanthanide systems. These results are summarized in Fig. 7. As the figure indicates, some compositions show coexistence of two phases according to X-ray powder diffraction.

Fig. 7 clearly illustrates a difference in behavior between the early and late lanthanide systems. The existence of the tetragonal Zr_5Si_4-type phase is restricted to the lighter, larger

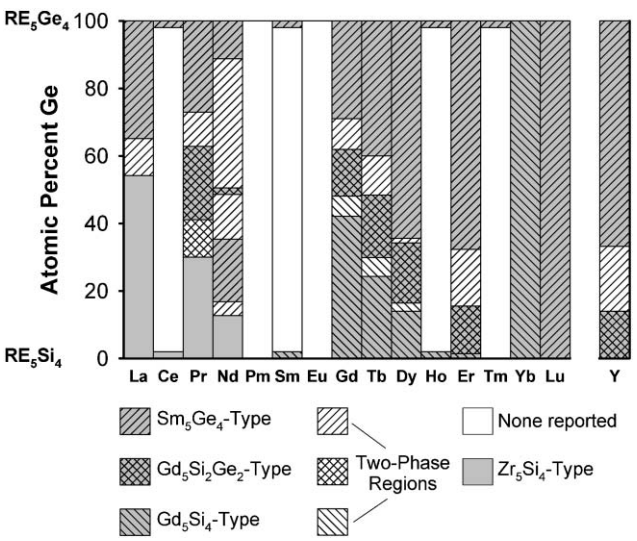

Fig. 7 Representation of the different room temperature crystal structures adopted by RE_5Tt_4 samples. Several regions (designated blank) have no structures reported. Gray shaded regions are single phase; unshaded regions are two-phase regions showing the two respective boundary phases.

† The orthorhombic Gd_5Si_4-type and Sm_5Ge_4-type structures are isopointal, *i.e.*, they are described by the same space group, *Pnma*, and have identical asymmetric units. However, the arrangement of atoms in the two unit cells gives distinctly different sets of interatomic distances that suggest different chemical bonding scenarios in the two structure types.

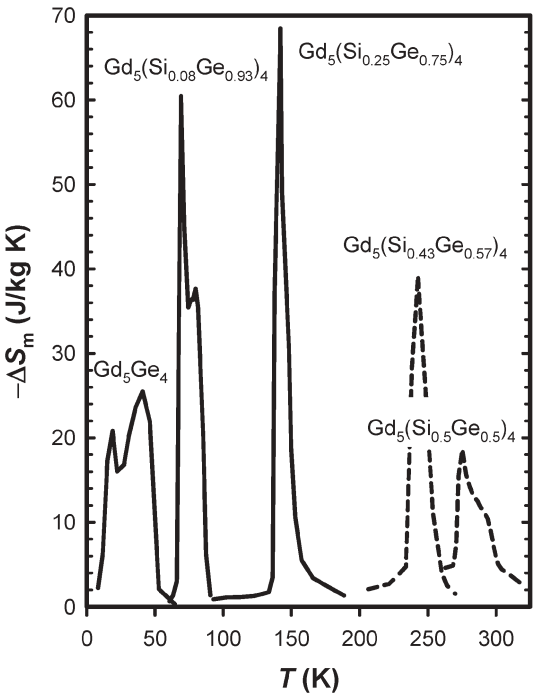

Fig. 8 The MCE characteristic, $-\Delta S_m(T, \Delta H = 5\ T)$ curves, for various $Gd_5(Si_xGe_{1-x})_4$. Data for this figure come from ref. 9.

lanthanide examples. The Gd-, Tb- and Dy-systems show similar features, but the Curie temperatures are largest for the Gd samples and the stability window for the Sm_5Ge_4-type structure increases along the period. Calorimetric and magnetic measurements indicate giant MCE in these systems when there is a change in crystal structure from either the Sm_5Ge_4-type or $Gd_5Si_2Ge_2$-type to the Gd_5Si_4-type, and the Gd systems show the widest temperature range for such applications. Fig. 8 illustrates $-\Delta S_m(T)$ curves for various Ge-rich $Gd_5(Si_xGe_{1-x})_4$. Since their Curie temperatures span *ca*. 250 K, different $Gd_5(Si_xGe_{1-x})_4$ will be effective magnetocaloric materials for different temperature ranges.[9] Furthermore, the Ge-rich $Gd_5(Si_xGe_{1-x})_4$ samples show significantly larger isothermal magnetic entropy changes near their corresponding Curie temperatures than other rare-earth intermetallics.[9] A great deal of research into understanding the behavior of these materials has focused on thorough crystallographic and magnetic studies coupled with electronic structure calculations. Before such experiments can be conducted, however, appropriate samples free of impurities are necessary—"first comes the synthesis!"

Synthetic and thermodynamic issues

Since all component elements have high melting points, these rare-earth compounds are typically prepared by arc-melting the reactants followed by annealing under inert atmospheres or in high vacuum to improve the phase purity of the product. The choice of reaction container, purity of the starting elements, and annealing times affect the quality of the product, as seen in the MCE as characterized by the isothermal entropy change.[26] Much of the effort to date to optimize synthetic conditions has emphasized $Gd_5Si_2Ge_2$ due to its favorable Curie temperature for near ambient refrigeration applications. When commercial Gd is used to prepare $Gd_5Si_2Ge_2$, the MCE is approximately 2.5 times smaller than that obtained when Ames Laboratory Gd is used. Commercial Gd purities can range from 90–98 atomic percent with O, N, C and H atoms as the major impurities. Gd prepared in the Ames Laboratory is 99.8 atomic percent pure, with *ca*. 400 ppm O, 200 ppm C, and 200 ppm H. High purity Si and Ge are readily available. Commercially available rare-earth elements contain impurity levels that are sufficiently high to impede the magnitude of the MCE. A comparison of MCE by ΔS_m in $Gd_5Si_2Ge_2$ prepared with high purity Gd and the addition of 10 molar percent carbon produced identical features to the sample prepared with commercial Gd. However, the mechanism of this effect is not clear.[27]

High temperature annealing is best performed in tantalum or tungsten ampoules. Since tantalum is easier to work, it is the material of choice. Niobium and molybdenum react with the starting materials, as does yttria-stabilized zirconia and alumina. However, prolonged heating of silicides in tantalum ampoules give Ta_2Si as a by-product, especially for large reaction samples. This results in lower Si content in the final $RE_5(Si_xGe_{1-x})_4$ products. In the Gd system, $Gd_5Si_2Ge_2$ and Gd_5Ge_4 melt incongruently at, respectively, 2020 $\pm$ 25 and 1960 K while Gd_5Si_4 melts congruently at *ca*. 2070 K, so there can be segregation during precipitation of ternary samples. In fact, high temperature experiments and analysis of MCE from $Gd_5Si_2Ge_2$ samples cut from the final product reveal that Si-rich products solidify first followed by Ge-rich products, so there can be a concentration gradient of Si (Ge) in the final product, which will impact the observed MCE.[26]

Lower temperature annealing of $Gd_5(Si_xGe_{1-x})_4$ ($0.4 \leqslant x \leqslant 0.503$) shows evidence for eutectoid decomposition into $Gd_5(Si_xGe_{1-x})_3$ and $Gd(Si_xGe_{1-x})$.[15] The phase diagram suggests this decomposition for Gd_5Si_4 below 923 K, so care is required to obtain pure, single phase materials suitable for bulk physical property measurements and applications. As we have already mentioned, monoclinic $Gd_5Si_2Ge_2$ appears to be metastable at room temperature by transforming under mild heat treatment into the Gd_5Si_4-type when annealed between 670 and 970 K, but the transformation is sufficiently slow that the monoclinic structure remains for heat treatments below 600 K. Presently, optimum heat treating is short (*ca*. one hour) annealing at *ca*. 1300 °C, which also leads to a partial redistribution of Si and Ge atoms among their crystallographic sites.[28] Large single crystals can also be grown by the Bridgman method.[29] As the chemistry and properties of $Gd_5(Si_xGe_{1-x})_4$ and other $RE_5(Si_xGe_{1-x})_4$ are strongly tied to their crystal structures, we now focus on this.

Structural specifics and transitions for MCE materials

Among the $RE_5(Si_xGe_{1-x})_4$ systems, those showing giant MCE involve the three structure types observed in the Gd system as noted in Fig. 7. All three are constructed from the same building block: a quasi-infinite, two-dimensional slab of composition RE_5Tt_4 (here, Tt = (Si_xGe_{1-x}) mixture). From a network perspective, each slab consists of two, eclipsed

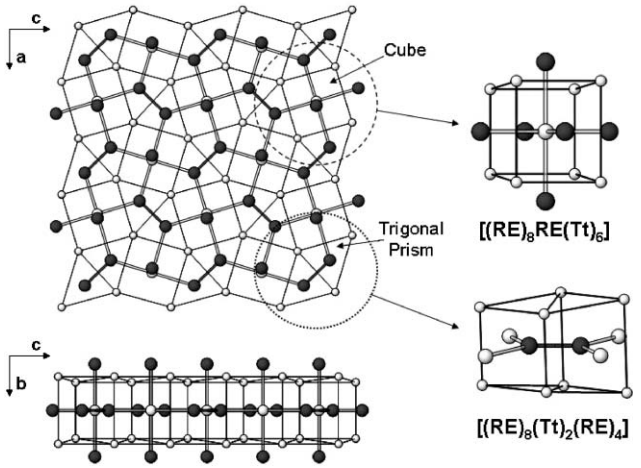

Fig. 9 Important structural building blocks of the giant MCE materials in RE_5Tt_4. Open circles are RE sites; dark circles are Tt sites. (Left) Network view of the $[RE_5Tt_4]$ two-dimensional slab: (Top) projection along the **b**-axis emphasizing the eclipsed 3^2434 nets formed by the RE atoms and the cubic and trigonal prismatic holes formed by these two planes. (Bottom) projection along the **a**-axis emphasizing the layered nature and the Tt atoms protruding above and below the slabs. (Right) Two important cluster units that build up these structures. The relationship between the slabs and these clusters is highlighted.

3^2434 nets of RE atoms, which give rise to cubic and trigonal prismatic holes, shown in Fig. 9. In each cubic hole sits another RE atom, while a Tt atom occupies every trigonal prismatic hole. As the trigonal prisms share a common rectangular (vertical) face, these Tt atoms actually form Tt–Tt dimers with distances in the range 2.55–2.64 Å. These distances are within the range of single-bonded Tt–Tt contacts. To complete the stoichiometry, the square faces top and bottom are capped by additional Tt atoms. From the perspective of clusters, each slab is a 1 : 1 condensation of two distinct units: (1) a RE atom surrounded by a cube of eight RE atoms and an octahedron of six Tt atoms, *i.e.*, $[(RE)_8RE(Tt)_6]$; and (2) a Tt–Tt dimer with each Tt atom coordinated by a trigonal prism of RE atoms and the open rectangular faces capped by RE atoms, *i.e.*, $[(RE)_8Tt_2(RE)_4]$.

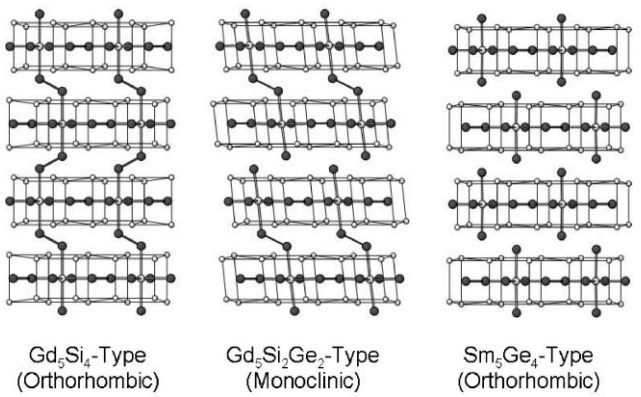

Fig. 10 Three different structure types of the giant MCE materials in RE_5Tt_4 viewed along their crystallographic **a**-axes. (Left) the orthorhombic Gd_5Si_4-type; (Middle) the monoclinic $Gd_5Si_2Ge_2$-type; and (Right) the orthorhombic Sm_5Ge_4-type. Tt–Tt bonds less than 3.0 Å are noted by solid lines and RE–Tt bonds in the cubic-octahedral cluster are noted by open lines.

The three structure types are differentiated by how the slabs are connected to each other, as shown in Fig. 10: (i) in the Gd_5Si_4-type, there are short (single-bonded) Tt–Tt contacts between the slabs; (ii) in the Sm_5Ge_4-type, the Tt–Tt contacts between the slabs exceed 3.5 Å and are essentially nonbonding; and (iii) in the monoclinic $Gd_5Si_2Ge_2$-type, planes of Tt–Tt contacts between slabs alternate between bonding (*ca.* 2.6 Å) and nonbonding (*ca.* 3.5 Å). The monoclinic structure, therefore, is intermediate between the Gd_5Si_4-type and the Sm_5Ge_4-type. Both orthorhombic structure types crystallize in the space group *Pnma* but with distinctly different *b*/*a* and *c*/*a* ratios of the unit cell parameters: these ratios are larger for the Gd_5Si_4-type examples.[30] The space group for the monoclinic structure is $P112_1/a$, which is a proper subgroup of *Pnma*. Therefore, the temperature-dependent transformations between these different structure types (see Fig. 6) can be viewed as the relative, cooperative shear motion of the slabs. Between the Gd_5Si_4-type and Sm_5Ge_4-type observed for Ge-rich $Gd_5(Si_xGe_{1-x})_4$ samples, alternate slabs shift in opposite directions along the crystallographic *a*-axis. Between the monoclinic $Gd_5Si_2Ge_2$-type and Gd_5Si_4-type seen in $Gd_5Si_2Ge_2$, alternating *pairs of slabs* shift in opposite directions along the *a*-axis. As Fig. 6 also illustrates, these structural changes accompany magnetic order–disorder transitions and contribute to giant MCE in these systems.

The asymmetric units of the orthorhombic structures contain three RE sites (RE1 and RE2 as the 3^2434 nets; RE3 within the cube) and three Tt sites (Tt1 is between slabs forming Tt1–Tt1 contacts; Tt2 and Tt3 are within slabs forming Tt2–Tt3 dimers). For the monoclinic structure, there are nine atoms in the asymmetric unit with the RE1 and RE2 sites each splitting into two pairs (RE1a, RE1b and RE2a, RE2b) and the Tt1 site also splitting into a pair of distinct sites (Tt1a, Tt1b). These different crystallographic sites allow numerous chemical substitution patterns and exploration of relationships between chemical composition, structure and properties.

In the $Gd_5(Si_xGe_{1-x})_4$ system, in particular, accurate determinations of Tt site occupancies show that Si and Ge atoms are not distributed completely randomly throughout the structure, as might be expected. In fact, Ge atoms tend to build up between slabs in the so-called Tt1 sites while Si atoms prefer sites within the slabs at Tt2 and Tt3. Reasons for this segregation involve both size and electronegativity arguments. The interslab Tt1 sites are better suited for larger atoms, while electronic structure calculations suggest that among the three Tt sites, the Tt1 position shows the greatest attraction for the more electronegative main group element.[30] As the electronegativities of the Group 14 elements increase along the sequence Sn–Si–Ge while the size increases along Si–Ge–Sn, current research is exploring $Gd_5(Si_xSn_{1-x})_4$ and $Gd_5(Ge_xSn_{1-x})_4$ to elucidate factors influencing this site preference issue. Nonetheless, a semi-quantitative thermodynamic analysis based upon calculated total electronic energies for different colorings of $Gd_5Si_2Ge_2$ nicely confirms the observed distribution of Si and Ge atoms, where enthalpy factors influence an ordered, segregated arrangement while

entropy factors at high temperature drive disordered, random arrangements. There are also some interesting observations concerning structural changes in $Gd_5(Si_xGe_{1-x})_4$ at room temperature as x varies: (i) the Gd_5Si_4-type phases with Tt1–Tt1 bonds exist when the fraction of Si_2 dimers exceeds Ge_2 dimers at the Tt1–Tt1 sites; and (ii) the Sm_5Ge_4-type phases with no Tt1–Tt1 bonds exist when the fraction of Ge_2 dimers exceeds both SiGe and Si_2 dimers at the Tt1–Tt1 sites. Therefore, the changes in Tt1–Tt1 bonding in $Gd_5(Si_xGe_{1-x})_4$ follow trends in bond strengths, $D(Ge_2) < D(SiGe) < D(Si_2)$, and the distribution of Si and Ge atoms greatly influences the structural behavior and, thus, the magnetic character of these materials.

In all three structure types, the Tt atoms occupy face-sharing trigonal prisms (see Fig. 9). The approximate site symmetry of the Tt2–Tt3 dimer is D_{2h}, while that for the Tt1–Tt1 dimer is C_{2h}. In addition to the changes in Tt1–Tt1 distances with structure type, a thorough analysis of interatomic contacts reveals other, significant distance changes between the Gd_5Si_4- and Sm_5Ge_4-types, which involve Tt1–RE1 and RE1–RE2 contacts between slabs. These are illustrated in Fig. 11, which shows trends in important distances between slabs as a function of x in $Gd_5(Si_xGe_{1-x})_4$. There is a Gd1–Gd2 contact between slabs that drops from *ca.* 3.8 Å in the Gd_5Si_4-type structures with short Tt1–Tt1 bonds to *ca.* 3.5 Å in the Sm_5Ge_4-type structures with long Tt1–Tt1 contacts, which contributes to the antiferromagnetic behavior of the Sm_5Ge_4-type compounds. In general, as the Tt1–Tt1 bond breaks in going from the Gd_5Si_4-type to the Sm_5Ge_4-type structure with decreasing x, the slabs tend to move closer together as Tt1–Tt1 bonds are replaced by Tt1–RE and RE–RE bonds, which is also reflected in lower b/a ratios in going from the Gd_5Si_4-type to the Sm_5Ge_4-type.[30] These changes have a profound effect on the physical properties of these systems through distinct changes in chemical bonding, which will be addressed in a later section.

During early studies of the transition in $Gd_5Si_2Ge_2$ between the low-temperature, ferromagnetic, Gd_5Si_4-type α-phase and

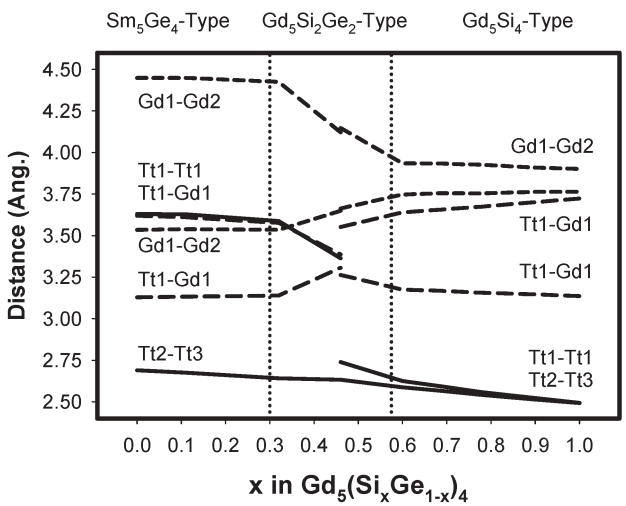

Fig. 11 Trends in significant interatomic distances for $Gd_5(Si_xGe_{1-x})_4$ plotted as a function of Si concentration x. Solid lines represent Tt–Tt distances; dashed lines represent Tt–Gd and Gd–Gd distances between slabs emphasized in Figs. 9 and 10.

the room-temperature, paramagnetic, monoclinic β-phase, the question arose whether the Tt1–Tt1 bonds remaining in the β-phase could be broken by further heating. Such a transition would result in the Sm_5Ge_4-type structure for $Gd_5Si_2Ge_2$. Indeed, at 593 K β-$Gd_5Si_2Ge_2$ transforms into an orthorhombic, paramagnetic γ-phase according to both high temperature, single crystal X-ray diffraction and magnetic measurements, but, surprisingly, the Tt1–Tt1 distances are all *ca.* 2.73 Å.[31] This result places the γ-phase into the Gd_5Si_4-type regime, which means that the Tt1–Tt1 bonds reform on heating! Although theoretical predictions suggested that this β–γ transition could be accompanied by an irreversible redistribution of Si and Ge atoms, the diffraction experiments showed that the Si and Ge atom distributions remain constant for the entire temperature range studied. On cooling, electron microscopy and X-ray diffraction indicate that both monoclinic β- and orthorhombic γ-phases coexist at room temperature, while a magnetization study on a crystal of $Gd_5Si_2Ge_2$ revealed the Curie temperature of the orthorhombic γ-phase to be *ca.* 298 K. Therefore, the $Gd_5Si_2Ge_2$ is extraordinarily complex with three transitions characterized: (i) ferromagnetic to paramagnetic (''second-order'') α–γ transition at 298 K; (ii) ferromagnetic to paramagnetic (''first-order'') α–β transition at 272 K; and (iii) paramagnetic to paramagnetic (''first-order'') β–γ transition at 593 K. Furthermore, the nature of these transitions can be further complicated by adventitious interstitial atoms, like O or N.

At present, most efforts exploring phase transitions in RE_5Tt_4 have concentrated on Gd systems, but Tb[21] and Dy[25] systems are increasingly studied. Overall, these systems undergo magnetic and structural transitions under changing temperatures and compositions as well as magnetic fields. $Tb_5Si_2Ge_2$ is particularly interesting because of the existence of a ferromagnetic, monoclinic phase below 114 K before the monoclinic–orthorhombic, Gd_5Si_4-type transition at 105 K, which represents the first magnetically ordered monoclinic phase observed in RE_5Tt_4.[32] The case of Er_5Si_4 indicates that structural and magnetic transitions need not be coupled to one another.[33] Paramagnetic Er_5Si_4 undergoes a first-order structural transition from high-temperature, orthorhombic Gd_5Si_4-type to low-temperature, monoclinic $Gd_5Si_2Ge_2$-type between 200 and 230 K with no change in magnetic order. Ferromagnetic order sets in at 32 K, which is characterized as second-order according to calorimetric measurements. Neutron diffraction results obtained using a different Er_5Si_4 sample (prepared from a commercial grade Er) indicate an orthorhombic, Gd_5Si_4-type structure (Tt1–Tt1 distance of 2.60 Å) both above and below 32 K,[34] which points to the absence of the high temperature, structural-only transformation and highlights extreme sensitivity of this system to impurity levels. Furthermore, the effect of magnetic field can be studied by *in situ* X-ray powder diffraction, and was demonstrated in Gd_5Ge_4.[18] In the absence of the external field, Tt1–Tt1 distances between slabs are 3.68 Å, but shorten to 2.70 Å when a 3.5 Tesla field is applied. Cooling Gd_5Ge_4 in the absence of a field does not drive the identical transition at temperatures as low as 2 K. Thus, RE_5Tt_4 allow for numerous investigations of structure–property relationships.

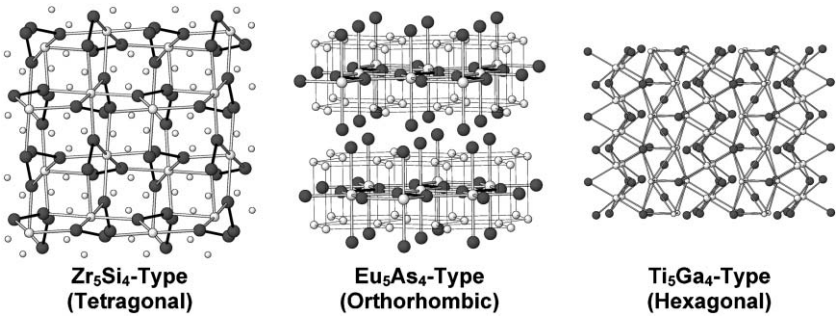

Fig. 12 Three important structure types that occur for other M_5X_4 systems related to RE_5Tt_4. (Left) The tetragonal Zr_5Si_4-type; (Middle) the orthorhombic Eu_5As_4-type; and (Right) the hexagonal Ti_5Ga_4-type. The metal sites are smaller, open circles; the main group atom sites are shaded circles.

As a final comment about structural specifics for RE_5Tt_4, the two most common competing structures that are encountered include the tetragonal Zr_5Si_4-type and the hexagonal Ti_5Ga_4-type, which are illustrated in Fig. 12. As we have already mentioned (see Fig. 7), the tetragonal structure is observed for the larger, lighter lanthanides, Si-rich systems. Although there are no slabs in the Zr_5Si_4-type structure, all Tt atoms belong to Tt–Tt dimers, just as in the orthorhombic Gd_5Si_4-type structures. From the structural point of view, any transition between the Zr_5Si_4-type and the orthorhombic Sm_5Ge_4- or Gd_5Si_4-types will be quite disruptive to the sample and may, in fact, be irreversible. $Pr_5Si_2Ge_2$ is reported in two modifications, monoclinic α-form and tetragonal β-form, depending upon the heat treatment of initially arc-melted mixture of elements, but no report of any structural transition exists.[35] Therefore, temperature-dependent studies are warranted. The hexagonal competitor, the Ti_5Ga_4-type, may also be described as a stuffed version of the hexagonal Mn_5Si_3 structure type, with the additional main group atom in an octahedral hole of the majority component. Since RE_5Tt_3 systems adopt the Mn_5Si_3-type structure and are frequently side products during the preparation of RE_5Tt_4, this hexagonal system is an important competing system to understand. This structure is observed for RE_5Tt_3Tt' samples, when the size of Tt exceeds that of Tt′, *e.g.*, as in Gd_5Sn_3Si.[36] A monoclinic structure type, the $U_2Mo_3Si_4$-type, is another possibility for RE_5Tt_4 systems, in which the Tt1–Tt1 dimers would be entirely equivalent, unlike in the monoclinic $Gd_5Si_2Ge_2$-type.[37] Although there have been no reports to date, recent unpublished work reveal this structure does manifest itself in ternary examples for mixtures of rare-earth elements. Finally, recent results from the study of new ternary rare-earth intermetallics in $RE_5Sb_2Si_2$ have uncovered the orthorhombic Eu_5As_4-type as another possible competing structure.[38] Here, there are short Si–Si dimers, but nonbonding Sb···Sb dimers.

Selected magnetic and physical properties

Fig. 8 illustrates the MCE for Ge-rich $Gd_5(Si_xGe_{1-x})_4$ systems. The maximum values of $|\Delta S_m|$ at the corresponding Curie temperatures are significantly larger than competing intermetallic compounds, so the designation "giant MCE materials" has been assigned to this system. Furthermore, during coupled magnetic–structural transitions, only the total change in entropy is measured, but there are entropy changes associated with both the change in magnetic order as well as for the structural transition. Various estimates of the entropy change associated with the structural transition in $RE_5(Si_xGe_{1-x})_4$ systems are 70–74 mJ cm^{-3} K^{-1} (*ca.* 1.1 J mol^{-1} K^{-1} or 9.3 J kg^{-1} K^{-1}).[9] According to Fig. 8, $|\Delta S_m|$ tends to increase as the Ge content increases (x decreases), and goes through a maximum value of *ca.* 68 J kg^{-1} K^{-1} at 145 K for $Gd_5(Si_{0.25}Ge_{0.75})_4$ before dropping to *ca.* 20 J kg^{-1} K^{-1} at 25 K for Gd_5Ge_4. According to eqn (6), this trend can be explained by (1) a tendency toward larger $|\Delta S_m|$ values as T_C drops; (2) the structural transitions that involve making or breaking just 50% of the Tt1–Tt1 bonds for the monoclinic phases at $x = 0.43$ and 0.50, but 100% Tt1–Tt1 bonds for the orthorhombic phases at $x = 0.25$, 0.0825 and 0 will give larger $|\Delta S_m|$ values to the Ge-rich samples due to larger enthalpy changes; and (3) as the Ge concentration increases, the fraction of weaker Ge–Ge dimers in the Tt1–Tt1 sites increases leading to smaller $|\Delta S_m|$ values. In addition to a giant MCE, many examples also exhibit extraordinary magnetostriction and magnetoresistance. For $Gd_5(Si_xGe_{1-x})_4$, the sign of magnetoresistance is negative, which implies lower

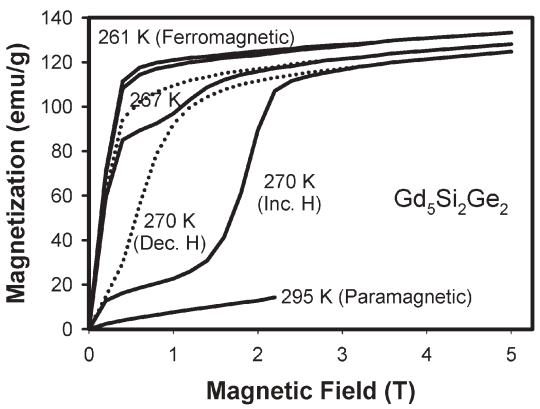

Fig. 13 Magnetization (emu g^{-1}) *vs.* magnetic field isotherms for $Gd_5Si_2Ge_2$ at temperatures both below and above the Curie temperature of 276 K. Above T_C, magnetization shows linear behavior with small fields ($H < 2.5$ T). Well below T_C, saturation is rapid. For intermediate temperatures near T_C, the existence of two phases, ferromagnetic and paramagnetic, has been used to explain the observed behavior.

resistivity (larger conductivity) for the low temperature phases, *i.e.*, the ferromagnetic, orthorhombic phases. Furthermore, magnetization measurements under different field strengths reveal the coexistence of two magnetic phases and, thus, the first-order nature of the transition in general.[8] Fig. 13 shows this behavior for $Gd_5Si_2Ge_2$. For temperatures above the Curie point, 276 K, the magnetization shows linear behavior under small applied fields. Below the Curie point, small fields lead to near saturation behavior, and the trend agrees with 20 (4f)[7] Gd atoms in the unit cell. Studying this material during both increasing and decreasing magnetic fields shows the coexistence behavior.

All RE_5Tt_4 systems studied thus far show metallic behavior with resistivities on the order of 0.1–100 mΩ cm. However, Gd_5Ge_4 shows an interesting metal–semiconductor transition at *ca*. 130 K, which is close to the Neél temperature for this phase.[39] In general, the extraordinary physical properties of these materials are linked to their magnetic structures. Therefore, several RE_5Tt_4 binary systems have been studied by neutron diffraction below magnetic ordering temperatures to show ferromagnetic ordering for orthorhombic Gd_5Si_4-type phases. The magnetic moments of the rare-earth atoms tend to align perpendicular to the stacking direction of the slabs, *i.e.*, perpendicular to the crystallographic *b*-axis. Although most structural information is known about the $Gd_5(Si_xGe_{1-x})_4$ systems, magnetic structures of Gd systems are unfortunately not easily obtained by neutron diffraction because Gd atoms scatter neutrons incoherently. Recent experiments utilizing X-ray resonant magnetic scattering on Gd_5Ge_4 below the Néel temperature of *ca*. 127 K have shown magnetic moments aligned along the crystallographic *c*-direction.[40] In this magnetic structure, the exchange coupling between Gd moments within slabs is ferromagnetic, while the coupling between slabs is antiferromagnetic: ferromagnetic Gd-rich slabs stack antiferromagnetically along the crystallographic *b*-direction. The Tb–Si–Ge system has been carefully studied between 2 K and 300 K to identify local magnetic moments at the Tb sites.[21] In this case there is evidence for canted ferromagnetic order and there are subtle changes in the orientation of the magnetic moments without changes in the gross magnetic behavior. Through a combination of neutron diffraction and magnetization measurements, a *T*–*x* phase diagram was proposed that resembles the Gd–Si–Ge diagram shown in Fig. 6. However, the ability to examine local magnetic structures by neutron diffraction for Tb allowed identification of a second magnetic-only transition.

Chemical bonding and electronic structure

It is the common hypothesis that observable physical phenomena are related to the electronic structure of a particular system. The challenges associated with the RE_5Tt_4 systems involve not only the temperature-dependent nature of the problem of the MCE, but also the complexity of these structures. Nevertheless, simple chemical models based upon structure can provide insights to explain features of the electronic structure and to provide chemical interpretation of the physical behavior. For giant MCE materials, RE_5Tt_4, there are three characterized structures. In all cases, we can treat the rare-earth element as formally trivalent, RE^{3+}. Since the interatomic distances observed for Tt–Tt dimers fall either within the range for single-bonded dimers or beyond van der Waals contacts, there are two distinct bonding schemes according to the Zintl–Klemm formalism (octet rule): (i) single bonded Tt–Tt dimers are isoelectronic with halogen dimers, *i.e.*, 14 valence electron $(Tt_2)^{6-}$ units; and (ii) nonbonded Tt···Tt dimers are isoelectronic with two isolated noble gas atoms, *i.e.* two 8 valence electron Tt^{4-} units. In the nonbonded dimer, the additional two valence electrons would occupy the σ_p* antibonding orbital and break the Tt–Tt bond. Thus, we can formulate the Gd_5Si_4-type structure for RE_5Tt_4 as $(RE^{3+})_5(Tt_2)^{6-}{}_2\cdot 3e^-$ as all Tt atoms are part of Tt–Tt single-bonded dimers (see Fig. 10). In order to achieve an electrically neutral chemical species, there are three valence electrons in excess. From the chemical perspective, these electrons would be assigned to valence 6s or 5d based orbitals from the RE atom and may be involved in RE–RE bonding; from the physical perspective, these electrons would be assigned to the conduction band. In the Sm_5Ge_4-type structure, 50% of the Tt atoms are part of single-bonded dimers, 50% are not, so the formalism becomes $(RE^{3+})_5(Tt_2)^{6-}(Tt^{4-})_2\cdot 1e^-$, which leads to a single excess valence electron. For the intermediate monoclinic $Gd_5Si_2Ge_2$-type structure, we have $(RE^{3+})_5(Tt_2)^{6-}{}_{1.5}(Tt^{4-})\cdot 2e^-$, and an intermediate number of excess valence electrons. Therefore, as transformations occur among different pairs of structures, we can envision an internal reduction–oxidation process in the solid-state: as Tt–Tt dimers are reduced, these electrons are formally transferred from the conduction band into the σ_p* antibonding orbital of the Tt–Tt dimer so that the Tt–Tt distance expands toward nonbonded values, and *vice versa*.[41]

The theoretical electronic structures, as expressed by the energy densities of states (DOS) curves, reflect these qualitative formulations for RE_5Tt_4 systems. Fig. 14 illustrate the non-spin-polarized DOS curves for Gd_5Si_4 in the Gd_5Si_4-type, $Gd_5Si_2Ge_2$ in the monoclinic $Gd_5Si_2Ge_2$-type and Gd_5Ge_4 in the Sm_5Ge_4-type structures. In these plots, the RE 4f orbitals are not plotted, as they remain typically well localized and are not involved in chemical bonding or significant interatomic orbital interactions. In $Gd_5Si_2Ge_2$, the Ge atoms are placed exclusively at the Tt1 sites and the Si atoms are at the Tt2 and Tt3 sites, which is the lowest energy arrangement. With 31 valence electrons per formula unit, the Fermi level occurs at nonzero DOS values, so both structures are expected to be metallic. The lowest lying valence orbitals, seen in the range *ca*. 10 eV below the Fermi level, are particularly diagnostic for the nature of Tt–Tt interactions: when only Tt–Tt single bonded dimers are present, as in Gd_5Si_4, then we see two peaks for the σ_s and σ_s* orbitals of the dimers. When the Tt···Tt linkage between slabs is nonbonding, then a third peak emerges between these two, which are essentially the Tt valence s atomic orbitals associated with these sites due to the coalescence of the σ_s and σ_s* orbitals of the dimer because the orbital interaction is much weaker than in the short dimers. The next set of states occurs *ca*. 5 eV below the Fermi energy, and constitutes a mixture of Tt valence p atomic orbitals with Gd 6s and 5d orbitals. For Gd_5Si_4, there is a gap in the DOS curve at 28 valence electrons, which corresponds exactly to the

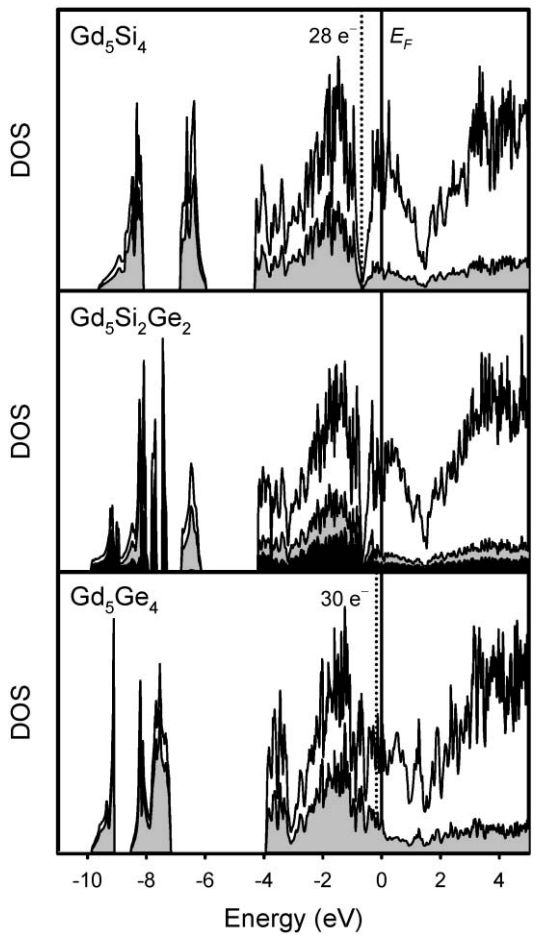

Fig. 14 DOS curves for (top) Gd_5Si_4, (middle) $Gd_5Si_2Ge_2$ and (bottom) Gd_5Ge_4 showing just the valence electron region within a 15 eV surrounding the corresponding Fermi levels. Energies are relative to the Fermi level of each system. Shaded regions correspond to Si and/or Ge levels contributing to the total DOS curve. For Gd_5Si_4, a deep pseudogap is seen for states containing 28 electrons per formula; for Gd_5Ge_4, no such pseudogap is seen for states containing 30 electrons per formula (see corresponding dotted lines).

formal electron counting of the two Si–Si dimers in the chemical formula. For Gd_5Ge_4, the energy gap at 28 valence electrons is lost, but there is a significant minimum at 30 valence electrons because the Ge–Ge σ_p* orbital for the Tt1–Tt1 sites drops in energy due to the long interatomic separation. In the case of $Gd_5Si_2Ge_2$, the DOS curve is further complicated by the different orbital energies (electronegativities) of Si and Ge, but the qualitative features of the binary examples remain. All three examples, nevertheless, indicate that states around the Fermi level have mostly Gd 5d and 6s contributions. Furthermore, analysis of specific orbital interactions around the Fermi levels indicates significant occupation of Tt–Tt antibonding orbitals, which is partially compensated by bonding overlap with Gd 5d and 6s orbitals.[42] The Tt–Tt antibonding orbitals are a mixture of π* and σ_p* orbitals, but consistent with the notion that these dimers are formally isoelectronic with halogen dimers, for which the highest occupied molecular orbitals would be the π* levels. Nevertheless, it seems that the RE_5Tt_4 structures gain some stability by occupying states in excess of what is needed by the main group (Tt) elements alone.[43]

The $Yb_5(Si_xGe_{1-x})_4$ is an excellent system to analyze the relationship between electronic structure, chemical bonding and geometrical structure.[24] Least squares fits to magnetization data in the Curie–Weiss regime for several samples yield an average effective moment per Yb atom of 2.79 μ_B, which is much smaller than the theoretical free ion effective moment of Yb^{3+}, 4.54 μ_B. This result is taken as evidence for mixed valent behavior of Yb involving Yb^{2+} (μ_{eff} = 0) and Yb^{3+}. Averaging the results over several samples gives the fraction of Yb^{3+} in $Yb_5(Si_xGe_{1-x})_4$ is *ca.* 40% and of Yb^{2+} is *ca.* 60%. Therefore, the number of valence electrons assigned to $Yb_5(Si_xGe_{1-x})_4$ is close to 28 valence electrons, which matches the number of valence electrons needed to fill the orbitals associated with two Tt–Tt dimers in the chemical formula. In line with this qualitative argument, and the bonding analysis of the DOS curves, $Yb_5(Si_xGe_{1-x})_4$ adopt the Gd_5Si_4-type structures for all x with Tt1–Tt1 distances ranging between 2.5 and 2.6 Å.

X-ray photoelectron spectra for $Gd_5(Si_xGe_{1-x})_4$ show a broad maximum at energies 1.5–2.0 eV below the Fermi level, which has been attributed to Gd 5d–(Si, Ge) sp covalently bonding states, in agreement with the calculated DOS curves.[44] Moreover, the spectra for the three specific cases, Gd_5Si_4, $Gd_5Si_2Ge_2$ and Gd_5Ge_4, differ in the range 0–1.0 eV below Fermi: (i) Gd_5Si_4 shows a bump at *ca.* 0.7 eV; (ii) $Gd_5Si_2Ge_2$ shows a similar feature, but at 0.3 eV; while (iii) this feature is hardly visible for Gd_5Ge_4. The changing electronic structures due to the changing nature of chemical bonding within Tt1–Tt1 dimers between slabs gives rise to these variations, which are nicely verified by the calculated electronic structures.

There is a clear correlation between the concentration of conduction electrons and the preferred magnetic exchange interactions in the RE_5Tt_4 systems: (i) the Gd_5Si_4-type structures with formally *three* conduction electrons per formula unit show ferromagnetic behavior; and (ii) the Sm_5Ge_4-type structures with formally *one* conduction electron per formula unit show antiferromagnetic behavior. Except for $Tb_5Si_2Ge_2$, where a ferromagnetic region has been reported, all monoclinic $Gd_5Si_2Ge_2$-type structures undergo either a structural (as in Er_5Si_4) or a coupled structural–magnetic transition before the onset of magnetic order. Variations in preferred magnetic exchange interactions do correlate with the concentration of valence electrons, as seen in transition metals as well as in $GdCu_{1-x}Zn_x$. The Ruderman–Kittel–Kasuya–Yosida (RKKY) model was applied to understand the indirect exchange coupling between Gd sites in $Gd_5(Si_xGe_{1-x})_4$ by using the calculated density of conduction electrons and Fermi wavevectors for each of the three systems: Gd_5Si_4, $Gd_5Si_2Ge_2$ and Gd_5Ge_4.[16] The result was surprisingly consistent with observations, although the free-electron model on which the RKKY model is based seems inappropriate for these compounds, as can be seen in their calculated DOS curves. Subsequently, first principles calculations of the total effective exchange coupling, which made use of the local spin density approximation, verified the changing exchange coupling with Fermi level and showed that it is short-ranged, dropping quickly after a single lattice translation.[42] Therefore, experiments and theory are in agreement that the magnetic coupling

within each RE_5Tt_4 slab is ferromagnetic, whereas there can be different couplings between slabs depending on the nature of their mutual interactions. When the Tt–Tt interaction is strong between slabs, the exchange prefers ferromagnetic ordering; when the Tt–Tt is weak between slabs, exchange prefers antiferromagnetic ordering. Such calculations have been used to calculate free energies and magnetizations *vs.* temperature and magnetic field, and have successfully interpreted the giant MCE in the $Gd_5(Si_xGe_{1-x})_4$ system.[42]

Substitutional chemistry

The structures adopted within the RE_5Tt_4 family of compounds are sufficiently robust to allow chemical substitutions that affect both the unit cell sizes and the concentrations of valence electrons. When these substitutions are successful, they can provide information about the relationships among chemical composition, geometrical, electronic and magnetic structures and physical properties for this family. As a brief reminder, the three structure types involved with the giant MCE in RE_5Tt_4 essentially involve three different kinds of RE sites and three different kinds of Tt sites, so that both ordered and disordered substitutional variants are possible. Furthermore, the RE_5Tt_4 system shows a maximum 31 valence electrons per formula unit when we consider just the valence 6s and 5d electrons from the RE elements. Also, $Gd_5(Si_xGe_{1-x})_4$ shows that there can be one to three electrons, formally, in the conduction band per formula unit, which leads to different structural behavior. Mixed valence behavior of Yb in $Yb_5(Si_xGe_{1-x})_4$ suggests that 28 valence electrons per formula unit can be achieved with structural implications as well. Therefore, chemical substitutions in these systems have predicted behavior with respect to structural features, atomic distributions and properties.

Substitution for RE atoms: Fig. 7 indicates the broad capability for these structures to be formed by the rare-earth elements. There have been a few reports of mixed rare-earth systems, which keep the systems isoelectronic. However, when structural characterization has relied exclusively on X-ray powder diffraction data, there have been no reports of an ordering among the three different crystallographic sites, although the RE1 site shows the largest volume among the three RE sites. A recent single crystal study of "$RE_2RE'_3Si_4$" silicides did show partial segregation of the smaller rare-earth element into RE3 (preferentially) and RE2 sites, with a small amount into the RE1 site.[45] Changing the rare-earth element for metal atoms with different valence, *e.g.*, monovalent or divalent elements, has been attempted with some success in maintaining the structure. There has been a report of Tb_4LiGe_4, with Li substituting for Tb.[38] In this case, the Ge–Ge (Tt1–Tt1) distance between the slabs is short, leading to the Gd_5Si_4-type structure. Since Tb_4LiGe_4 has 29 valence electrons per formula as compared to 31 electrons for Sm_5Ge_4-type Tb_5Ge_4, the change in structure that accompanies the change in number of valence electrons can be explained by a reduction of electrons occupying the Tt1–Tt1 σ_p* orbital. In the DOS, the lower electron count would affect the position of the Fermi level to depopulate antibonding states within the Tt1–Tt1 dimer. Another set of examples include $La_{5-x}Ca_xGe_4$ ($3.4 \leqslant x \leqslant 3.8$) and $Ce_{5-x}Ca_xGe_4$ ($3.0 \leqslant x \leqslant 3.3$).[46] In these, the divalent element Ca has a similar size to the rare-earth element. However, these examples show one astounding characteristic: their numbers of valence electrons drop below 28 electrons. This observation apparently contradicts the notion that the stability of Sm_5Ge_4-type structures relies on some additional conduction electrons beyond a Zintl threshold.[43]

Attempts to substitute magnetic rare-earth elements by smaller, nonmagnetic elements like Na, Mg, Al or In have led to structures with features similar to the orthorhombic RE_5Tt_4 phases. Many adopt the U_3Si_2-type structure,[41] *e.g.*, Gd_2MgGe_2 and Gd_2InGe_2, which also show differing magnetic behavior based upon the numbers of valence electrons. The crystal structure of the tetragonal U_3Si_2-type structure involves identical slabs to those found in orthorhombic RE_5Tt_4 systems, but they are condensed and stack quasi-infinitely along the *c*-axis. Substitution of Al for Gd created a new structure-type, the Gd_2AlGe_2-type with some unusual structural features.[41]

Substitution for Tt atoms: Substitution at the tetrelide atoms is also possible, and allows for variable electron counts. The greatest success has occurred with Ga for Ge, which creates challenges to identify Ga and Ge using single crystal X-ray diffraction.[47] Nevertheless, since Ga has one less valence electron than Ge, $Gd_5(Ga_xGe_{1-x})_4$ were predicted to show structural effects based primarily on changes in valence electron count and minimally on size effects. Experimental results indicated that the maximum concentration of Ga to replace Ge is $x = 0.55$, while the Tt1–Tt1 distance in room temperature structures showed a significant drop when x exceeded 0.25, *i.e.* Gd_5GaGe_3. Trends in interatomic distances for $Gd_5(Ga_xGe_{1-x})_4$ are shown in Fig. 15. If Fig. 15 is compared to Fig. 11, there are significant similarities to the changes in structure influenced by size and electronegativity of Si and to those influenced by the concentration of valence electrons of Ga. Theoretical calculations place Ge atoms

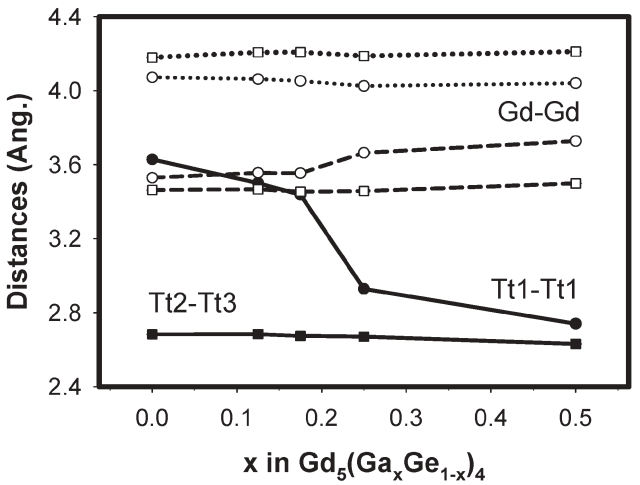

Fig. 15 Trends in interatomic distances for $Gd_5(Ga_xGe_{1-x})_4$ plotted as a function of Ga concentration x. Only Tt–Tt and Gd–Gd distances are shown, to emphasize the significant change in Tt1–Tt1 distance with x.

preferentially at the Tt1 sites, but this awaits experimental confirmation.[47] Further studies using Sn, P and Sb substituents have also revealed structural impacts, but characterization is limited to X-ray powder diffraction. Nevertheless, in general, as electron-poorer elements like Ga replace Ge in Sm_5Ge_4-type RE_5Ge_4, Tt1–Tt1 bonds gradually form between the slabs; as electron-richer elements like P replace Si in Gd_5Si_4-type RE_5Si_4, Tt1–Tt1 bonds break. Furthermore, increasing the size of the Tt atom, *e.g.* by replacing Si or Ge with Sn, the Tt1–Tt1 bonds tend to break, at least for room temperature structures.

Outlook for room temperature applications

A near room temperature reciprocating magnetic refrigerator was designed and built by Astronautics Corporation of America in collaboration with the Ames Laboratory.[4] This refrigerator achieved a cooling power of 600 Watts in a 5 Tesla magnetic field over a temperature span of 10 K (the temperature difference between the hot and cold heat exchangers). The device achieved a Carnot efficiency approaching 75% and used 3.0 kg commercial grade Gd spheres as the refrigerant. Since then, more than 10 near room temperature magnetic refrigerators have been built and tested.[9] In addition to various engineering and technological issues, there are numerous concerns about refrigerant materials, which include cost, environmental impacts, hysteresis associated with first-order phase transitions, time-dependences of ΔT_{ad}, and corrosion. Nevertheless, one advantage of magnetic refrigeration is that these applications rely on bulk properties. Therefore, identifying materials that will show consistent and reproducible effects at cost-effective and environmentally-benign means are the significant goals and challenges.

Summary

The RE_5Tt_4 systems provide tremendous potential for applications but also exceptional capacity for fundamental studies in solid-state chemistry and physics. Structure and properties can be modified significantly by changes in composition, temperature, pressure and magnetic fields. Enormous chemical and physical flexibility can be achieved by this system through chemical substitutions, compositional variation, heating and cooling, and magnetic fields. RE_5Tt_4 are a tremendous scientific ''playground'' for chemists, physicists and materials scientists and continue to provide enormous opportunities for probing structure–composition–property–bonding relationships.

Acknowledgements

The author wishes to thank Wonyoung Choe, Sean McWhorter, Sumohan Misra, Yurij Mozharivskyj, Eric Poweleit, and Alexandra Tsokol for contributing substantially to the scientific content of this work. The author also acknowledges Karl Gschneidner, Vitalij Pecharsky, Bruce Harmon, German Samolyuk, Vladimir Antropov, Tom Lograsso, Scott Chumbley, David Jiles for numerous discussions about this project. And, the author thanks Dr Yuri Grin and colleagues at the Max-Planck-Institute für Chemische Physik fester Stoffe for providing resources to complete this review. The Ames Laboratory is operated by Iowa State University for the US Department of Energy (DOE) under contract No. W-7405-ENG-82. This research was supported by the Office of Basic Energy Sciences, Materials Sciences Division of the US DOE.

References

1 W. R. Woolrich, *The Men Who Created Cold; A History of Refrigeration*, Exposition Press, New York, 1962.
2 W. Gumprecht, ''Refrigerants of the 21st Century, Part 3. Early Refrigerants,'' http://www.chemcases.com/fluoro/fluoro03.htm.
3 G. S. Nolas, J. Sharp and H. J. Goldsmid, *Thermoelectrics: Basic Principles and New Materials Development*, Springer, Berlin, 2001.
4 C. Zimm, A. Jastrab, A. Sternberg, V. Pecharsky, K. Gschneidner, Jr., M. Osborne and I. Anderson, ''Description and performance of a near room temperature magnetic refrigerator'', *Adv. Cryog. Eng.*, 1998, **43**, 1759–1766.
5 V. K. Pecharsky and K. A. Gschneidner, Jr.,''Magnetocaloric Effect,'', in *Encyclopedia of Condensed Matter Physics*, Elsevier, Amsterdam, 2005, pp. 236–244.
6 V. K. Pecharsky and K. A. Gschneidner, Jr., ''Magnetocaloric Effect and Magnetic Refrigeration'', *J. Magn. Magn. Mat.*, 1999, **200**, 44–56.
7 M. E. Zhitomirsky, ''Enhanced magnetocaloric effect in frustrated magnets'', *Phys. Rev. B: Condens. Matter*, 2003, **67**, 1–7, 104421/1–7.
8 K. A. Gschneidner, Jr. and V. K. Pecharsky, ''Magnetocaloric Materials,'', *Ann. Rev. Mater. Sci.*, 2000, **30**, 387–429.
9 K. A. Gschneidner, Jr., V. K. Pecharsky and A. O. Tsokol, ''Recent Developments in Magnetocaloric Materials'', *Rep. Prog. Phys.*, 2005, **68**, 1479–1539.
10 C. P. Bean and D. S. Rodbell, *Phys. Rev.*, 1961, **126**, 104.
11 P. J. von Ranke, N. A. de Oliveira, C. Mello, A. M. G. Carvalho and S. Gama, ''Analytical Model to Understand the Colossal Magnetocaloric Effect'', *Phys. Rev. B*, 2005, **B71**, 054410/1–6.
12 V. K. Pecharsky and K.A. Gschneidner, Jr., ''Giant Magnetocaloric Effect in $Gd_5Si_2Ge_2$'', *Phys. Rev. Lett.*, 1997, **78**, 4494–4497.
13 O. Tegus, E. Brück, L. Zhang, K. H. J. Dagula and F. R. de Boer Buschow, ''Magnetic-Phase Transitions and Magnetocaloric Effects'', *Physica B (Amsterdam)*, 2002, **319**, 174–192.
14 F. Holtzberg, R. J. Gambino and T. R. McGuire, ''New Ferromagnetic 5:4 Compounds in the Rare Earth Silicon and Germanium Systems'', *J. Phys. Chem. Solids*, 1967, **28**, 2283–2289.
15 A. O. Pecharsky, K. A. Gschneidner, Jr., V. K. Pecharsky and C. E. Schindler, ''The Room Temperature Metastable/Stable Phase Relationships in the Pseudo-Binary Gd_5Si_4-Gd_5Ge_4 System, *J. Alloys Compd.*, 2002, **338**, 126–135.
16 W. Choe, V. K. Pecharsky, A. O. Pecharsky, K. A. Gschneidner, Jr., V. G. Young, Jr. and G. J. Miller, ''Making and Breaking Covalent Bonds Across the Magnetic Transition in the Giant Magnetocaloric Material, $Gd_5(Si_2Ge_2)$'', *Phys. Rev. Lett.*, 2000, **84**, 4617–4620.
17 Ya. Mudryk, Y. Lee, T. Vogt, K. A. Gschneidner, Jr. and V. K. Pecharsky, ''Polymorphism of $Gd_5Si_2Ge_2$: The Equivalence of Temperature, Magnetic Field, and Chemical and Hydrostatic Pressures'', *Phys. Rev. B: Condens. Matter*, 2005, **B71**, 174104/1–6.
18 V. K. Pecharsky, A. P. Holm, K. A. Gschneidner, Jr. and R. Rink, ''Massive Magnetic-Field-Induced Structural Transformation in Gd_5Ge_4 and the Nature of the Giant Magnetocaloric Effect'', *Phys. Rev. Lett.*, 2003, **91**, 197204/1–4.
19 L. Morellon, J. Blasco, P. A. Algarabel and M. R. Ibarra, ''Nature of the First-Order Antiferromagnetic-Ferromagnetic Transition in the Ge-Rich Magnetocaloric Compounds $Gd_5(Si_xGe_{1-x})_4$'', *Phys. Rev. B: Condens. Matter*, 2000, **B62**, 1022–1026.
20 W. Choe, G. J. Miller, J. Meyers, S. Chumbley and A. O. Pecharsky, '''Nanoscale Zippers' in the Crystalline Solid. Structural Variations in the Giant Magnetocaloric Material $Gd_5Si_{1.5}Ge_{2.5}$'', *Chem. Mater.*, 2003, **15**, 1413–1419.

21 C. Ritter, L. Morellon, P. A. Algarabel, C. Magen and M. R. Ibarra, ''Magnetic and Structural Phase Diagram of $Tb_5(Si_xGe_{1-x})_4$'', *Phys. Rev. B: Condens. Matter*, 2002, **B65**, 094405/1–10.

22 A. O. Pecharsky, K. A. Gschneidner, Jr., V. K. Pecharsky, D. L. Schlagel and T. A. Lograsso, ''Phase Relationships and structural, magnetic, and thermodynamic properties of alloys in the pseudobinary Er_5Si_4-Er_5Ge_4 system'', *Phys. Rev. B: Condens. Matter*, 2004, **B70**, 144419/1–11.

23 A. O. Pecharsky, V. K. Pecharsky and K. A. Gschneidner, Jr., ''Phase relationships and low temperature heat capacities of alloys in the Y_5Si_4-Y_5Ge_4 pseudo binary system'', *J. Alloys Compd.*, 2004, **379**, 127–134.

24 K. Ahn, A. O. Tsokol, Yu. Mozharivskyj, K. A. Gschneidner, Jr. and V. K. Pecharsky, ''Phase Relationships and Structural, Magnetic, and Thermodynamic Properties of the Yb_5Si_4–Yb_5Ge_4 Pseudobinary System'', *Phys. Rev. B: Condens. Matter Mater. Phys.*, 2005, **B72**, 054404/1–11.

25 K. A. Gschneidner, Jr., V. K. Pecharsky, A. O. Pecharsky, V. V. Ivtchenko and E. M. Levin, ''The Nonpareil $R_5(Si_xGe_{1-x})_4$ Phases'', *J. Alloys Compd.*, 2000, **303–304**, 214–222.

26 K. A. Gschneidner, Jr., A. O. Pecharsky, V. K. Pecharsky, T. A. Lograsso and D. L. Schlagel, ''Production of the Giant Magnetocaloric Effect $Gd_5(Si_xGe_{1-x})_4$ Magnetic Refrigerant Materials from Commercial Gadolinium Metal'' in *Rare Earths and Actinides: Science, Technology and Applications IV*, ed. R. G. Bautista and B. Mishra, The Minerals, Metals and Materials Society, 2000, pp. 63–72.

27 K. A. Gschneidner, Jr. and V. K. Pecharsky, ''Magnetic Refrigeration Materials'', *J. Appl. Phys.*, 1999, **85**, 5365–5368.

28 A. O. Pecharsky, K. A. Gschneidner, Jr. and V. K. Pecharsky, ''The Giant Magnetocaloric Effect of Optimally Prepared $Gd_5Si_2Ge_2$'', *J. Appl. Phys.*, 2003, **93**, 4722–4728.

29 T. A. Lograsso, D. L. Schlagel and A. O. Pecharsky, ''Synthesis and Characterization of Single Crystalline $Gd_5(Si_xGe_{1-x})_4$ by the Bridgman Method'', *J. Alloys Compd.*, 2005, **393**, 141–146.

30 W. Choe, A. O. Pecharsky, M. Wörle and G. J. Miller, '''Nanoscale Zippers' in $Gd_5(Si_xGe_{1-x})_4$: Symmetry and Chemical Influences on the Nanoscale Zipping Action'', *Inorg. Chem.*, 2003, **42**, 8223–8229.

31 Y. Mozharivskyj, A. O. Pecharsky, V. K. Pecharsky and G. J. Miller, ''On the High-Temperature Phase Transition of $Gd_5Si_2Ge_2$'', *J. Am. Chem. Soc.*, 2005, **127**, 317–324.

32 L. Morellon, C. Ritter, C. Magen, P. A. Algarabel and M. R. Ibarra, ''Magnetic-martensitic transition of $Tb_5Si_2Ge_2$ studied with neutron powder diffraction'', *Phys. Rev. B: Condens. Matter Mater. Phys.*, 2003, **68**, 024417/1–6.

33 V. K. Pecharsky, A. O. Pecharsky, Y. Mozharivskyj, K. A. Gschneidner, Jr. and G. J. Miller, ''Decoupling of the Magnetic and Structural Transformations in Er_5Si_4'', *Phys. Rev. Lett.*, 2003, **91**, 207205/1–4.

34 J. M. Cadogan, D. H. Ryan, Z. Altounian, X. Liu and I. P. Swainson, ''Magnetic structure of Er_5Si_4'', *J. Appl. Phys.*, 2004, **95**, 7076–7078.

35 H. F. Wang, G. H. Rao, G. Y. Liu, Z. W. Ouyang, X. M. Feng, W. F. Liu, W. G. Chu and J. K. Liang, ''Structure dependence of magnetic properties of $Pr_5Si_2Ge_2$'', *J. Phys.: Condens. Matter*, 2002, **14**, 9705–9711.

36 Y. Mozharivskyj, A. O. Tsokol and G. J. Miller, ''Structural Variations in $Gd_5Si_{4-x}Sn_x$: Size vs. Electronic Effects'', *Z. Kristallogr.*, 2006, **221**, 5, in press.

37 K. W. Richter and H. F. Franzen, ''Structure-Composition Relations and Fractional Site Occupancy of New M_5Ge_4 Compounds in the System Ge–Ta–Zr'', *J. Solid State Chem.*, 2000, **150**, 347–355.

38 A. Yu Kozlov, V. V. Pavlyuk and V. M. Davydov, ''The Crystal Structure of the New Ternary Compounds $RE_5Sb_2X_2$ (RE – Y, Tb, Dy, Ho, Er, Tm; X – Si or Ge)'', *Intermetallics*, 2004, **12**, 151–155.

39 E. M. Levin, V. K. Pecharsky, K. A. Gschneidner, Jr. and G. J. Miller, ''The Electrical Resistivity, Electronic Heat Capacity and Electronic Structure of Gd_5Ge_4'', *Phys. Rev. B: Condens. Mat. Mater. Phys.*, 2001, **64**, 235103/1–11.

40 L. Tan, A. Kreyssig, J. W. Kim, A. I. Goldman, R. J. McQueeney, D. Wermeille, B. Sieve, T. A. Lograsso, D. L. Schlagel, S. L. Bud'ko, V. K. Pecharsky and K. A. Gschneidner, Jr., ''Magnetic Structure of Gd_5Ge_4,'', *Phys. Rev. B: Condens. Matter*, 2005, **71**, 214408/1–6.

41 G. J. Miller, C.-S. Lee and W. Choe, ''Structure and Bonding Around the Zintl Border,'', *Highlights in Inorganic Chemistry*, Ed. G. Meyer, Wiley-VCH, 2002, 21–54.

42 V. K. Pecharsky, G. D. Samolyuk, V. P. Antropov, A. O. Pecharsky and K. A. Gschneidner, Jr., ''The Effect of Varying the Crystal Structure on the Magnetism, Electronic Structure and Thermodynamics in the $Gd_5(Si_xGe_{1-x})_4$ System Near $x = 0.5$'', *J. Solid State Chem.*, 2003, **171**, 57–68.

43 A. Guloy and J. D. Corbett, ''Syntheses and structure of the La_5Ge_3Z phases (Z = Si, Sn, Pb, Ga, In): Structural relationships among the M_5X_4-type structures'', *J. Solid State Chem.*, 2005, **178**, 1112–1124.

44 G. Skorek, J. Deniszczyk and J. Szade, ''Electronic Structure of $Gd_5(Si, Ge)_4$'', *J. Phys.: Condens. Matter*, 2002, **14**, 7273–7286.

45 U. C. Rodewald, B. Heying, D. Johrendt, R.-D. Hoffmann and R. Pöttgen, ''Ternary Rare Earth Metal Silicides $RE_2RE'_3Si_4$ with Orthorhombic Sm_5Ge_4 or Tetragonal Zr_5Si_4 Type Structure'', *Z. Naturforsch. B: Chem. Sci.*, 2004, **59**, 174–181.

46 L.-M. Wu, S.-H. Kim and D.-K. Seo, ''Electronic-Precise/Deficient $La_{5-x}Ca_xGe_4$ ($3.4 \leqslant x \leqslant 3.8$) and $Ce_{5-x}Ca_xGe_4$ ($3.0 \leqslant x \leqslant 3.3$): Probing Low-Valence Electron Concentrations in Metal-Rich Gd_5Si_4-Type Germanides'', *J. Am. Chem. Soc.*, 2005, **127**, 15682–15683.

47 Yu. Mozharivskyj, W. Choe, A. O. Pecharsky and G. J. Miller, ''Phase Transformation Driven by Valence Electron Concentration: Tuning Interslab Bond Distances in $Gd_5Ga_xGe_{4-x}$'', *J. Am. Chem. Soc.*, 2003, **125**, 15183–15190.